Electronic Supplementary Information

Construction of a dephosphorylation-mediated chemiluminescent biosensor for multiplexed detection of DNA glycosylases in cancer cells

Ming-hao Liu,‡[a] Chuan-rui Wang,‡[a] Wen-jing Liu,‡[b] Xiao-rui Tian,‡[a] Qinfeng Xu,*[c] and Chun-yang Zhang*[a]

[a] College of Chemistry, Chemical Engineering and Materials Science, Shandong Normal University, Jinan 250014, China.

[b] School of Chemistry and Chemical Engineering, Southeast University, Nanjing 211189, China.

[c] School of Food and Biological Engineering, Shaanxi University of Science and Technology, Xi'an 710021, China

* Corresponding Authors: E-mail: cyzhang@sdnu.edu.cn; xuqinfeng@sust.edu.cn.

‡ These authors contributed equally.

Table S1. Sequences of the oligonucleotides [α]

Note	Sequence (5′-3′)
hAAG substrate	TTA ACT AAC TAC TAT GTC ACT ATG GTT CCC ACA AIG CTA GCT CAG TCA TAC ACG-PO_4
UDG substrate	TGG AGC ATA AGT AGG TTG TAT AGT TTA CCG TGT AUG ACT GAG CTA GCT TTG TGG-PO_4
biotin-labeled poly-(T) probe	TTT TTT TTT TTT TTT TTT TTT-biotin
capture probe A	TTG TGG GAA CCA TAG TGA CAT AGT AGT TAG TTA A-SH
capture probe B	TAC ACG GTA AAC TAT ACA ACC TAC TTA TGC TCC A-SH

[α] The underlined letter "I" indicates the deoxyinosine, and the underlined letter "U" indicates the deoxyuridine.

Emission Spectra of ALP-AMPPD Chemiluminescence System

The chemiluminescence signal was measured by a fluorescence spectrophotometer (FLS 1000, Edinburgh, UK). As shown in Fig. S1, a broad emission is observed in the region of 400–650 nm, with the maximum emission peak at 468 nm. This measured maximum emission peak is consistent with the reported value (470 nm).[1]

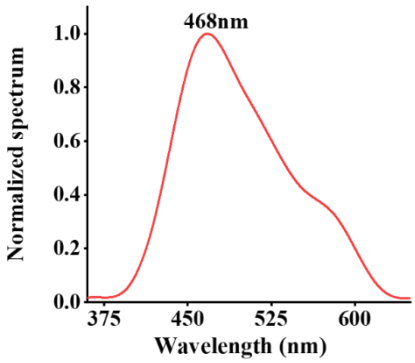

Fig. S1 Normalized emission (Em) spectra of ALP-AMPPD chemiluminescence system.

Molecular mechanism of DNA glycosylases-mediated cleavage of the bifunctional dsDNA substrate

Human alkyladenine DNA glycosylase (hAAG) is a mono-functional glycosylase specific for deoxyinosine base paired with a thymine.[2] As shown in Fig. S2A, hAAG specifically binds to DNA containing a target damaged base by inserting a β-hairpin loop into the minor groove of DNA. Glu125 acts as a general base to deprotonate a water molecule, which may serve as a nucleophile to attack the anomeric C1′ carbon in an S_N 2 catalytic mechanism. The hAAG can specifically recognize I:T base pairs and cleave the N-glycosidic bond between the deoxyribose and the hypoxanthine base, forming an AP site. Subsequently, APE1 cleaves on the 5′ side at AP site, forming a gap in the phosphodiester backbone with 3′-OH and 5′-deoxyribose-5-phosphate (dRP) ends. Consequently, in the presence of hAAG, the bifunctional dsDNA substrate can be specifically cleaved into two sections due to the combination of the glycosylase activity of hAAG and endonuclease activity of APE1.

The UDG is a mono-functional glycosylase specific for uracil base paired with a thymine as well. As shown in Fig. S2B, UDG specifically binds to DNA containing a target damaged base by inserting a β-hairpin loop into the minor groove of DNA. Asp145 acts as a general base to deprotonate a water molecule, which may serve as a nucleophile to attack the anomeric C1′ carbon in an S_N 2 catalytic mechanism. UDG can specifically recognize U:A base pairs and cleave the N-glycosidic bond between the deoxyribose and uracil base, forming an AP site. Subsequently, APE1 cleaves on the 5′ side at AP site, forming a gap in the phosphodiester backbone with 3′-OH and 5′-deoxyribose-5-phosphate (dRP) ends. Consequently, in the presence of UDG, the bifunctional dsDNA substrate can be specifically cleaved into two sections due to the combination of the

glycosylase activity of UDG and endonuclease activity of APE1.

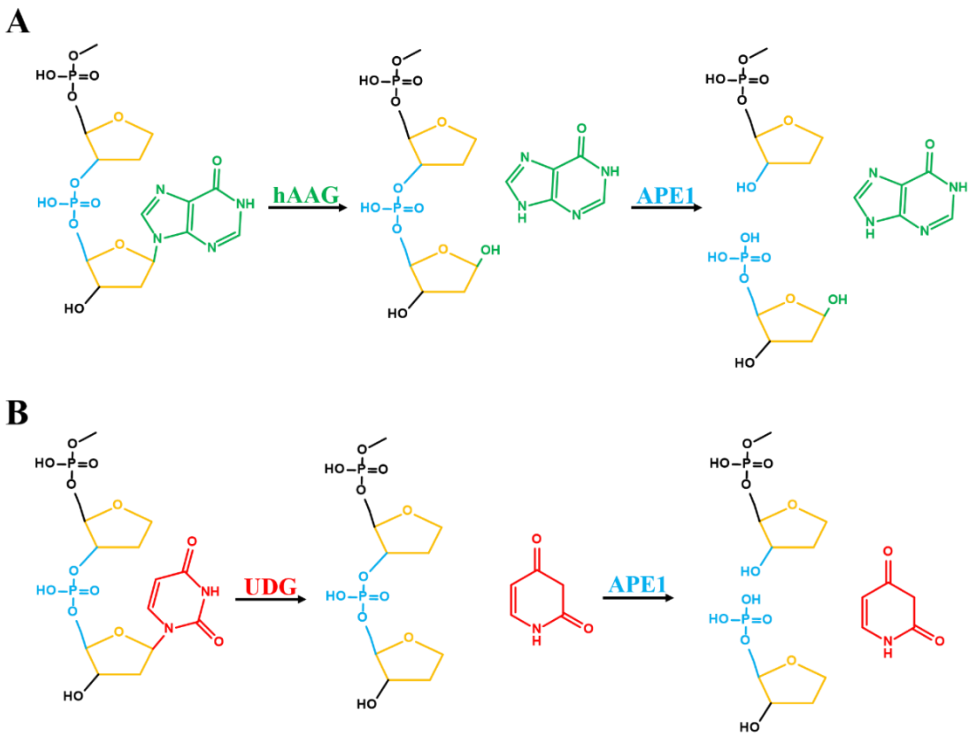

Fig. S2 (A) Mechanism of hAAG-mediated cleavage of the bifunctional dsDNA substrate with the assistance of APE1. The chemical steps of catalysis include step 1: removal of hypoxanthine (Hx) base and formation of AP site; step 2: cleavage of the phosphodiester bond on the 5′ side at the AP site. (B) Mechanism of UDG-mediated cleavage of the bifunctional dsDNA substrate with the assistance of APE1. The chemical steps of catalysis include step 1: removal of uracil base and formation of AP site; step 2: cleavage of the phosphodiester bond on the 5′ side at AP site.

Verification of the Construction of the AuNPs-dsDNA-biotin Nanostructures

We employed UV-vis absorption spectroscopy to confirm the successful construction of the AuNPs-dsDNA-biotin nanostructures. As shown in Fig. S3, in comparison with the AuNPs (Fig. S3, black line), both the AuNPs-dsDNA-biotin nanostructures A and B (Fig. S3, green and red line) have characteristic DNA peak at 260 nm and typical AuNPs peak at 520 nm with a slight

redshift because the attachment of dsDNA to the surface of AuNPs induces the change in nanoparticle size, particle aggregation, and local dielectric environments,[3] suggesting the successful assembly of dsDNA-biotin on the surface of AuNPs.

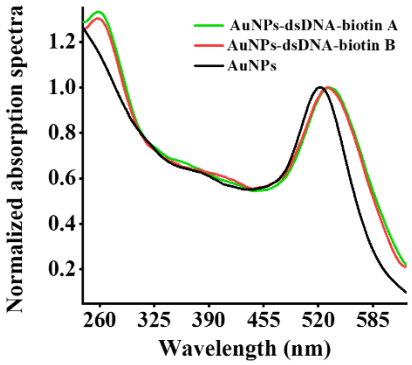

Fig. S3 Normalized UV-vis absorption spectra of AuNPs (black line), AuNPs-dsDNA-biotin nanostructure A (green line), and AuNPs-dsDNA-biotin nanostructure B (red line). The data of the characteristic absorption peaks of AuNPs were normalized.

Optimization of Experimental Conditions

To achieve the best assay performance, we optimized a series of experimental parameters including the concentration of bifunctional dsDNA substrate, the amount of TdT, the concentrations of biotin-labeled poly-(T) probe and SA-ALP. The concentration of the bifunctional dsDNA substrate is a crucial factor which influences the amplification efficiency of TdT-mediated polymerization reaction. On one hand, the high-concentration bifunctional dsDNA substrate can induce high amplification efficiency, but it might increase background signal as well. On the other hand, the low-concentration bifunctional dsDNA substrate can decrease the background signal, but it may cause low amplification efficiency. As shown in Fig. S4A, the $I - I_0$ values in rows A and B enhance with the increasing concentration of bifunctional dsDNA substrate from 150 to 250 nM, followed by the decrease beyond the concentration of 250 nM, respectively

(I and I_0 are the chemiluminescence intensity in the presence and absence of DNA glycosylases, respectively). Thus, 250 nM bifunctional dsDNA substrate is used in the subsequent researches.

In this assay, the concentration of TdT is critical for signal amplification, and thus the amount of TdT should be optimized. As shown in Fig. S4B, the $I - I_0$ values in rows A and B enhance with the increasing concentration of TdT from 0.2 to 0.3 U/μL and reaches a plateau at the concentration of 0.3 U/μL, respectively (I and I_0 are the chemiluminescence intensity in the presence and absence of DNA glycosylases, respectively). Therefore, 0.3 U/uL of TdT is used in the subsequent researches.

The concentration of biotin-labeled poly-(T) probe is directly related to the capture efficiency of ALP and the intensity of chemiluminescent signal, and thus the concentration of T-biotin probe should be optimized as well. As shown in Fig. S4C, the $I - I_0$ values in rows A and B enhance with the increasing concentration of biotin-labeled poly-(T) probe from 100 to 400 nM and reaches a plateau at 400 nM, respectively (I and I_0 are the chemiluminescence intensity in the presence and absence of DNA glycosylases, respectively). Therefore, 400 nM is used as the optimal biotin-labeled poly-(T) probe concentration.

We further optimized the amount of SA-ALP. ALP is critical in the chemiluminescent system, and it catalyzes the dephosphorylation of AMPPD to generate a chemiluminescence signal. As shown in Fig. S4D, the $I - I_0$ values in rows A and B enhance with the increasing amount of SA-ALP from 40 to 100 ng, and reaches a plateau at 100 ng, respectively (I and I_0 are the chemiluminescence intensity in the presence and absence of DNA glycosylases, respectively). Therefore, 100 ng of SA-ALP is used in the subsequent researches.

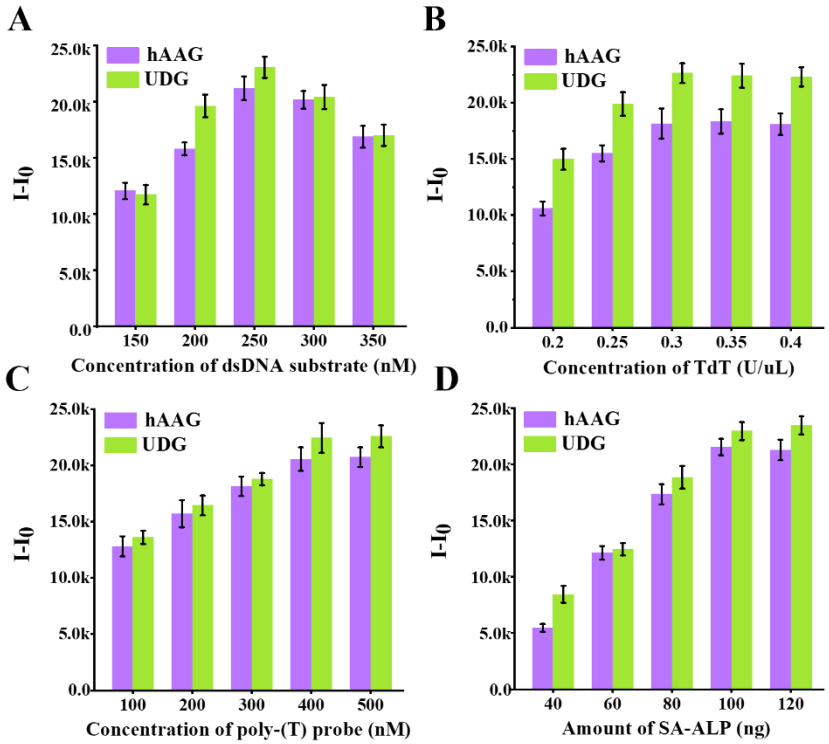

Fig. S4 (A) Variance of the $I - I_0$ value with different concentrations of bifunctional dsDNA substrate in the presence of hAAG (purple column) and UDG (green column), respectively. (B) Variance of the $I - I_0$ value with different concentrations of TdT in the presence of hAAG (purple column) and UDG (green column), respectively. (C) Variance of the $I - I_0$ value with different concentrations of biotin-labeled poly-(T) probe in the presence of hAAG (purple column) and UDG (green column), respectively. (D) Variance of the $I - I_0$ value with different amounts of SA-ALP in the presence of hAAG (purple column) and UDG (green column), respectively. The hAAG concentration is 0.1 U/μL and the UDG concentration is 0.1 U/μL. Error bars represent the standard deviations of three experiments.

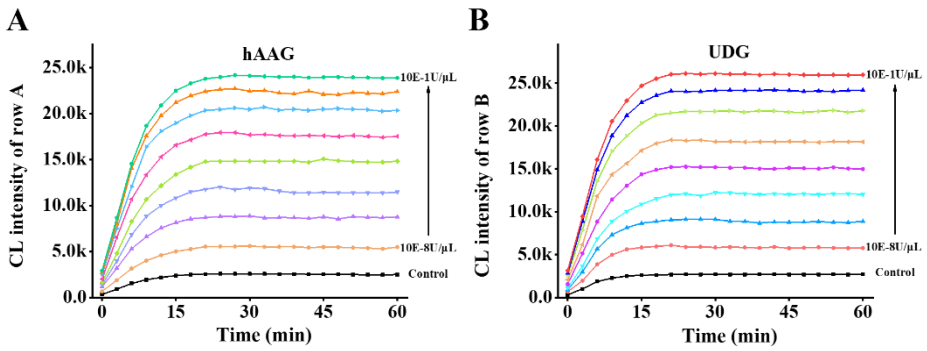

Fig. S5 (A) Real-time chemiluminescence signal in row A in response to different concentrations of hAAG. (B) Real-time chemiluminescence signal in row B in response to different concentrations of UDG.

We investigated the capability of this method for simultaneous detection of hAAG and UDG with different concentrations. For simultaneous analysis, the detection of DNA glycosylase with low concentration should not be interfered by other DNA glycosylases with high concentration. We first verified the effect of UDG with high concentration upon the detection of hAAG with low concentration. As shown in Fig. S6A, when the concentration of UDG is 0.1U/μL, the chemiluminescence intensity in row A improves gradually with the increasing concentration of hAAG from 1.0×10^{-8} to 1.0×10^{-5} U/μL (Fig. S6A, green column), consistent with the chemiluminescence intensity in row A generated by low hAAG concentration (1.0×10^{-8} – 1.0×10^{-5} U/μL) in the absence of UDG (Fig. S6A, purple column). Meanwhile, high chemiluminescence intensity in row B is measured in the presence of 0.1 U/μL UDG (Fig. S6A, orange column), suggesting that high concentration of UDG does not affect the detection of hAAG with low concentration. Similarly, when the concentration of hAAG is 0.1U/μL, the chemiluminescence intensity in row B improves gradually with the increasing concentration of UDG from 1.0×10^{-8} U/μL to 1.0×10^{-5} U/μL (Fig. S6B, pink column), consistent with the

chemiluminescence intensity in row B generated by low UDG concentration (1.0×10^{-8} – 1.0×10^{-5} U/μL) in the absence of hAAG (Fig. S6B, blue column). Meanwhile, high chemiluminescence intensity in row A is measured in the presence of 0.1U/μL hAAG (Fig. S6B, yellow column), suggesting that high concentration of hAAG does not affect the detection of UDG with low concentration.

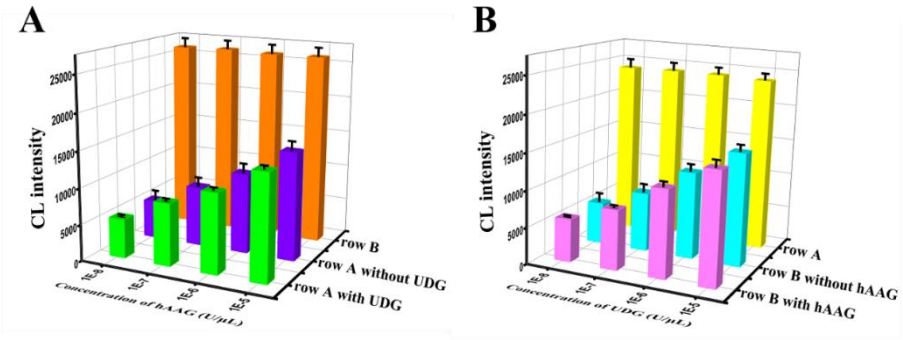

Fig. S6 (A) Chemiluminescence intensity in row A produced by different concentrations of hAAG from 1.0×10^{-8} to 1.0×10^{-5} U/μL in the presence (green column) and absence (purple column) of 0.1 U/μL UDG, and chemiluminescence intensity in row B produced by 0.1 U/μL UDG with different concentrations of hAAG (orange column). (B) Chemiluminescence intensity in row B produced by different concentrations of UDG from 1.0×10^{-8} to 1.0×10^{-5} U/μL in the presence (pink column) and absence (blue column) of 0.1 U/μL hAAG, and chemiluminescence intensity in row A produced by 0.1 U/μL hAAG with different concentrations of UDG (yellow column). Error bars represent the standard deviations of three experiments.

Simultaneous Detection of Multiple DNA Glycosylases in the Spiked Human Serum

To further evaluate the performance of the proposed method in real sample analysis, we measured the recovery ratios by spiking various-concentration hAAG (1×10^{-8} – 1×10^{-3} U/μL) and UDG (1×10^{-8} – 1×10^{-3} U/μL) into 10% human serum (Tables S2-3). As shown in Table S2,

the recovery ratio is determined to be 97.8–102.7% with a relative standard deviation (RSD) of 2.31–3.36% for hAAG, consistent with the value (recovery of 94.97–108.45% for hAAG) obtained by T7 transcription-driven symmetric amplification-based fluorescent assay.[4] As shown in Table S3, the recovery ratio is determined to be 98.3–101.5% with a RSD of 1.98–3.01% for UDG, in good agreement with the value (recovery of 98.06–103.93% for UDG) obtained by CRISPR-Cas12a amplification-based fluorescent assay.[5] These results demonstrate that the proposed method can be applied for simultaneous detection of multiple DNA glycosylases in complex biological samples.

Table S2. Recovery ratios of hAAG spiked in 10% human serum samples

Sample	Added (U/μL)	Determined (U/μL)	Recovery (%)	RSD (%)
1	1.0×10^{-3}	1.012×10^{-3}	101.2	2.54
2	1.0×10^{-5}	0.978×10^{-5}	97.8	2.31
3	1.0×10^{-8}	1.027×10^{-8}	102.7	3.36

Table S3. Recovery ratios of UDG spiked in 10% human serum samples

Sample	Added (U/μL)	Determined (U/μL)	Recovery (%)	RSD (%)
1	1.0×10^{-3}	0.991×10^{-3}	99.1	2.66
2	1.0×10^{-5}	0.983×10^{-5}	98.3	1.98
3	1.0×10^{-8}	1.015×10^{-8}	101.5	3.01

References

1. (a) L. Tu, Y. Wang, Y. Yang, B. H. Bakker, X. Kong, A. M. Brouwer, W. J. Buma and H. Zhang, *Phys. Chem. Chem. Phys.*, 2010, **12**, 6789-6794; (b) Z. Hai, J. Li, J. Wu, J. Xu and G. Liang, *J.*

Am. Chem. Soc., 2017, **139**, 1041-1044.

2. (a) D. M. Lyons and P. J. O'Brien, *J. Am. Chem. Soc.*, 2009, **131**, 17742-17743; (b) P. J. O'Brien and T. Ellenberger, *J. Biol. Chem.*, 2004, **279**, 9750-9757.

3. J. H. Choi and J. W. Choi, *Nano Lett.*, 2020, **20**, 7100-7107.

4. L.-j. Wang, L. Liang, B.-j. Liu, B. Jiang and C.-y. Zhang, *Chem. Sci.*, 2021, **12**, 5544-5554.

5. Y. C. Du, S. Y. Wang, Y. X. Wang, J. Y. Ma, D. X. Wang, A. N. Tang and D. M. Kong, *Biosens. Bioelectron.*, 2021, **171**, 112734.